BRAIN
ORIGINAL ARTICLE

Homomeric interactions of the MPZ Ig domain and their relation to Charcot-Marie-Tooth disease

Christopher P. Ptak,[1] Tabitha A. Peterson,[2] Jesse B. Hopkins,[3] Christopher A. Ahern,[2] Michael E. Shy[4] and Robert C. Piper[2]

Mutations in MPZ (myelin protein zero) can cause demyelinating early-onset Charcot-Marie-Tooth type 1B disease or later onset type 2I/J disease characterized by axonal degeneration, reflecting the diverse roles of MPZ in Schwann cells. MPZ holds apposing membranes of the myelin sheath together, with the adhesion role fulfilled by its extracellular immunoglobulin-like domain (Ig^{MPZ}), which oligomerizes.

Models for how the Ig^{MPZ} might form oligomeric assemblies has been extrapolated from a protein crystal structure in which individual rat Ig^{MPZ} subunits are packed together under artificial conditions, forming three weak interfaces. One interface organizes the Ig^{MPZ} into tetramers, a second 'dimer' interface links tetramers together across the intraperiod line, and a third hydrophobic interface that mediates binding to lipid bilayers or the same hydrophobic surface on another Ig^{MPZ} domain. Presently, there are no data confirming whether the proposed Ig^{MPZ} interfaces actually mediate oligomerization in solution, whether they are required for the adhesion activity of MPZ, whether they are important for myelination, or whether their loss results in disease.

We performed nuclear magnetic resonance spectroscopy and small angle X-ray scattering analysis of wild-type Ig^{MPZ} as well as mutant forms with amino acid substitutions designed to interrupt its presumptive oligomerization interfaces. Here, we confirm the interface that mediates Ig^{MPZ} tetramerization, but find that dimerization is mediated by a distinct interface that has yet to be identified. We next correlated different types of Charcot-Marie-Tooth disease symptoms to subregions within Ig^{MPZ} tetramers. Variants causing axonal late-onset disease (CMT2I/J) map to surface residues of Ig^{MPZ} proximal to the transmembrane domain. Variants causing early-onset demyelinating disease (CMT1B) segregate into two groups: one is described by variants that disrupt the stability of the Ig-fold itself and are largely located within the core of the Ig^{MPZ} domain; whereas another describes a region on the surface of Ig^{MPZ} tetramers, accessible to protein interactions. Computational docking studies predict that this latter disease-relevant subregion may potentially mediate dimerization of Ig^{MPZ} tetramers.

1 Biomolecular Nuclear Magnetic Resonance Facility, University of Iowa Carver College of Medicine, Iowa City, IA 52242, USA
2 Department of Molecular Physiology and Biophysics, University of Iowa Carver College of Medicine, Iowa City, IA 52242, USA
3 BioCAT, Department of Physics, Illinois Institute of Technology, Chicago, IL 60616, USA
4 Department of Neurology, University of Iowa Carver College of Medicine, Iowa City, IA 52242, USA

Correspondence to: Michael E. Shy
5-660 BSB, Molecular Physiology and Biophysics, University of Iowa, Iowa City, IA 52242, USA
E-mail: Michael-Shy@uiowa.edu

Received April 04, 2023. Revised June 28, 2023. Accepted July 17, 2023. Advance access publication August 5, 2023

Correspondence may also be addressed to: Robert C. Piper
E-mail: Robert-Piper@uiowa.edu

Keywords: peripheral neuropathy; myelin; cell adhesion; Charcot-Marie-Tooth

Introduction

Charcot-Marie-Tooth (CMT) disease refers to heritable peripheral neuropathies that affect 1:2500 individuals.[1] Most forms of CMT are demyelinating while one-third are primary axonal disorders.[2,3] Mutations in myelin protein zero (MPZ) account for 5% of CMT cases and can cause autosomal dominant demyelinating (CMT1B) or axonal degeneration (CMT2I/J), likely reflecting multiple molecular functions of MPZ in Schwann cells.[2,4]

MPZ comprises ~50% of the protein in myelin of the peripheral nervous and is critical for myelin function.[5,6] MPZ is a single-pass transmembrane protein with a single immunoglobulin-like (Ig) extracellular domain,[7,8] and cytosolic tail (Supplementary Fig. 1) that can be post-translationally modified by *N*-linked glycosylation, sulfation, palmitoylation and phosphorylation.[9,10] MPZ is an adhesion protein, holding together adjacent wraps of myelin membrane, which is thought to be mediated by homotypic interactions of its Ig domain.[11-13] The cytosolic tail of MPZ has a signalling role, promoting myelin compaction of the cytosolic region to form the major dense line.[12,14,15]

Exactly how the Ig domain of MPZ (Ig^{MPZ}) mediates adhesion of apposing membranes remains to be determined. Available models hypothesize that oligomerization of the Ig^{MPZ} mediates membrane adherence.[11-13] Yet, the potential interactions that support the MPZ oligomerization within the same membrane (*cis*) or across the intraperiod line (*trans*) have yet to be defined and verified biochemically.[12,14,15] Our current understanding for how the Ig^{MPZ} forms oligomerizes has been extrapolated from a protein crystal structure in which individual rat Ig^{MPZ} subunits were packed together under artificial conditions.[16] This showed two protein-protein interfaces: an asymmetric interface that drives the assembly of Ig^{MPZ} tetramers that would bundle four MPZ proteins embedded in the same membrane (a '*cis*' conformation); and a symmetrical dimeric interface bridging MPZs in apposing membranes (a '*trans*' conformation). While this model fits within the width of the intraperiod line that spans the gap between adhered membrane sheaths, crystal packing alone is an insufficient measure of how oligomerization occurs in solution. Indeed, another crystal structure of the human Ig^{MPZ} has a different crystal packing implying that the binding interfaces in the rat Ig^{MPZ} crystal lattice are not dominant drivers of oligomer assembly.[17] Recently, low resolution cryo-electron microscopic data from SDS-solubilized full-length MPZ led authors to propose a different configuration for how Ig^{MPZ} mediates adhesion,[18] namely that tetramers might not form but rather dimers in a *trans* conformation interact as a zipper to drive membrane adhesion. Finally, while CMT-causing variants within the Ig^{MPZ} are near the crystal packing interfaces,[19-22] there are no disease-causing variants known to precisely alter the surface residues of these interfaces. Together, these observations present two non-exclusive possibilities: (i) that the interfaces thought to control Ig^{MPZ} oligomerization are incorrect; and (ii) that the Ig^{MPZ} oligomerization is not strictly required for myelin function or that its interruption may not lead to a severe disease that would present clinically. One pathogenesis pathway that causes demyelinating CMT1B has been identified that involves accumulation of misfolded MPZ in the endoplasmic reticulum (ER), evoking ER-stress and activating the unfolded protein response (UPR).[23,24] However, not all disease-causing variants retain MPZ in the ER and/or cause ER stress suggesting there are other pathogenic mechanisms that may involve disrupting Ig^{MPZ} protein-protein interactions.[25]

To gain molecular insights into MPZ function, we performed solution binding studies to determine whether Ig^{MPZ} oligomerization is mediated through the interfaces identified with previous crystal packing data. We performed nuclear magnetic resonance (NMR) spectroscopy and small angle X-ray scattering (SAXS) analysis of wild-type Ig^{MPZ} as well as mutants with amino acid substitutions designed to interrupt its presumptive oligomerization interfaces. Our data confirm that the Ig^{MPZ} domain forms tetramers in solution. The Ig^{MPZ} also forms dimers, however, the mode of dimerization is inconsistent with current models and is mediated by an interface that remains to be identified. To provide a structural correlate for how distinct molecular mechanisms might drive CMT pathogenesis, we examined the molecular properties and location of disease-causing patient variants within the Ig^{MPZ} tetrameric structure. Here, we identified three spatially distinct residue groups. One group that causes severe early-onset demyelinating CMT1B maps to the core of the Ig^{MPZ} domain. Computational predictions show these variants destabilize the integrity of the Ig fold, consistent with previous studies showing many of these variants are retained in the ER and evoke the UPR. A second set of variants map to the perimeter of MPZ tetramers, potentially mediating interactions with other proteins such as MPZ from an apposing membrane. A third subregion mapping to a surface proximal to the transmembrane domain of the Ig^{MPZ} tetramer correlates with late-onset (CMT2I/J) in which myelin is mostly normal but axons degenerate.[26] Finally, we integrate a computational evaluation of disease-causing variants on the Ig^{MPZ} surface with alternative hypothetical oligomerization interfaces and discuss possibilities for how MPZ mediates adhesion of myelin layers and how its inability to do so might mediate different forms of CMT.

Materials and methods

Plasmids

The list of plasmids used for protein expression and how they were made is provided in Supplementary Table 1.

Protein expression and purification

The detailed method for production of Ig^{MPZ} is provided in the Supplementary material, 'Methods' section. Briefly, MBP-Ig^{MPZ} fusion proteins comprised of Maltose-binding protein, a TEV protease site, followed by an 'AASM' linker and residues I30-R153 of human MPZ was expressed in Origami 2(DE3) competent *Escherichia coli* (Novagen). MBP-Ig^{MPZ} was isolated from the periplasmic fraction generated by osmotic shock,[16] concentrated on DEAE-Sepharose fast flow resin (Amersham Biosciences), eluted and then isolated over amylose resin (New England Biolabs). Ig^{MPZ} was liberated from MBP-Ig^{MPZ} with tobacco etch virus (TEV) protease, followed by size-exclusion chromatography.

Nuclear magnetic resonance spectroscopy

NMR spectra were collected at 20°C on a Bruker AVANCE NEO 600 MHz NMR spectrometer with a gradient cryoprobe. $^{15}N/^{1}H$ heteronuclear single quantum correlation (HSQC) spectra were processed using NMRPipe[27] and analysed using POKY.[28] Longitudinal (T_1) and transverse (T_2) ^{1}H-detected 1D ^{15}N relaxation spectra were acquired on protein samples and relaxation curve-fitting analysis was performed with Topspin 4.0 (Bruker). For comparison with experimentally determined T_1/T_2 ratios, a theoretical T_1/T_2 ratio for the Ig^{MPZ} monomer was determined using HydroNMR[29] on NMRBox.[30]

Small angle X-ray scattering analysis

Ig^{MPZ} proteins were exchanged into SAXS buffer [50 mM NaCl, 1 mM EDTA, 20 mM TrisCl (pH 7.6)]. Ig^{MPZ} wild-type and W53A, R74A, D75R mutant were concentrated to 105 and 200 µM, respectively, and were subsequently diluted to 50–200 µM with SAXS buffer. Samples (50 µl) were centrifuged for 5 min at 13 000 rpm. SAXS was performed at BioCAT (beamline 18ID at the Advanced Photon Source) with in-line sample loading that was run at 0.3–0.4 ml/min on an AKTA Pure FPLC (GE) without column separation. The flow cell consisted of a 1.0 mm ID quartz capillary with ∼20 µm walls. A coflowing buffer sheath separated sample from the capillary walls to help prevent radiation damage.[31] Scattering intensity was recorded using an Eiger2 XE 9M (Dectris) detector placed 3.65 m from the sample giving access to a q-range of 0.003 $Å^{-1}$ to 0.34 $Å^{-1}$ (for wild-type) or 0.003 $Å^{-1}$ to 0.42 $Å^{-1}$ (for the W53A, R74A, D75R mutant). Exposures of 0.25 s were acquired every 0.5 s during elution.

Data were reduced using BioXTAS RAW 2.1.1.[32] I(q) versus q scattering curves were created from exposures selected from the sample peak. Matching buffer blanks for background subtraction were obtained from averaged presample exposures. The fraction of oligomers was determined from experimental SAXS data using the OLIGOMER program from the ATSAS suite.[33] Homo-oligomeric arrangements of Ig^{MPZ} were identified from the expanded unit cell of the Ig^{MPZ} crystal structure (PDB ID: 1NEU)[16] generated in UCSF Chimera.[34] To obtain theoretical form factors, structural predictions for the Ig^{MPZ} proteins were generated by a ColabFold[35] search of MMseqs2[36] with AlphaFold2.[37] Oligomeric arrangements were generated by superimposition of ColabFold Ig^{MPZ} structures onto crystal structure-derived Ig^{MPZ} oligomers.[38]

Fluorescence microscopy

HEK293 cells were grown on glass bottom dishes in Dulbecco's modified Eagle medium (Gibco) with 10% fetal bovine serum (Gibco) and 50 µg/ml penicillin/streptomycin at 37°C with 5% CO_2. Transfections were done in the absence of penicillin/streptomycin using Lipofectamine LTX Reagent with Plus Reagent (Invitrogen, Cat. No. A12621). Twenty-four hours post-transfection, live cell micrographs were captured using a Leica SP8 confocal microscope equipped with a 488 nm laser for excitation and an emission collection window of 520–540 nm.

Structural analysis

Crystal packing of the Ig^{MPZ} domain within 1NEU was examined using PISA.[39] Predictions on the effects of mutations on the interfaces predicted by the 1NEU crystal structure were made using SSIPe.[40] Calculating values for accessible surface area for each amino acid in the Ig^{MPZ} of 3OAI was done using UCSF Chimera.[34] Distance measurements and clash scores were also calculated using UCSF Chimera. Prediction of changes in the stability of the Ig^{MPZ} of 3OAI with different missense mutations was done using DeepDDG.[41] Generation and refinement of alternative Ig^{MPZ} dimer interfaces were done using ClusPro2.[42]

Results

Oligomerization interfaces for Ig^{MPZ}

The Ig^{MPZ} oligomerizes, which is thought to mediate adhesion of myelin wraps.[7] The interfaces hypothesized to mediate MPZ oligomerization have been extrapolated from a crystal structure of the rat Ig^{MPZ} wherein individual Ig^{MPZ} units form interfaces within the crystal lattice.[16] How these three interfaces are arranged to bridge Ig^{MPZ} across the intraperiod line are schematically shown in Fig. 1. One asymmetrical interface (Interface A) would mediate formation of Ig^{MPZ} tetramers in a parallel '*cis*' orientation emanating from the same membrane. A symmetrical dimer interface (Interface B) would link two apposing Ig^{MPZ} tetramers in antiparallel '*trans*' configuration that spans the ∼45 Å intraperiod line. A third interface (Interface C) from the crystal lattice highlights a tryptophan-containing hydrophobic patch that could mediate hydrophobic interactions with the apposing lipid bilayer. An alternate model (Fig. 1C) lacks Ig^{MPZ} tetramers and proposes that the dimer interface mediates interaction of two MPZ proteins in *trans* to zipper myelin wraps together.[18,20] Importantly, the interfaces in the rat Ig^{MPZ} crystal structure are predicted to be artefacts by PISA,[39] and there is a paucity of data corroborating these models for how Ig^{MPZ} oligomerizes.

Empirical testing of Ig^{MPZ} oligomerization interfaces

To investigate how Ig^{MPZ} oligomerizes in solution, we generated a recombinant soluble Ig^{MPZ} domain lacking the transmembrane and cytoplasmic regions of MPZ (Supplementary Fig. 1), which was analysed at various concentrations using NMR and SAXS. We also analysed mutant Ig^{MPZ} containing amino acid substitutions designed to disrupt Interface A (tetramer) alone, or in combination with disruption of Interface B (dimer). Interface A centres on W53 in one Ig^{MPZ} subunit, which is coordinated by H115, E97 and N116 on another Ig^{MPZ} subunit (Fig. 2A). Interface B defines a symmetric dimer held together by R74, D75 on one monomer engaging S78 on the other. Using a prediction algorithm,[40] we queried which different amino acid substitutions would cause the greatest change in binding energy at these interfaces without disrupting the integrity of the Ig fold itself (Fig. 2A and Supplementary Table 2). This identified the W53A mutation for disrupting Interface A (ΔA) and R74A, D75R mutations for disrupting Interface B (ΔB). None of these mutations have been reported in CMT patients, thus providing the basis of an unbiased structure/function analysis.

We then analysed ^{15}N-labelled wild-type Ig^{MPZ}, Ig^{MPZ}ΔA (W53A) and Ig^{MPZ}ΔAΔB (W53A, R74A, D75R) domains in NMR $^{15}N/^{1}H$ HSQC experiments (Fig. 2B and C and Supplementary Fig. 2). All produced similar well dispersed spectra of backbone amides indicating all three Ig^{MPZ} domains were well-folded. In the context of full-length MPZ with a C-terminal tagged GFP, both wild-type and the ΔAΔB mutant were found primarily at the cell surface of transiently transfected HEK293 cells, indicating each had folded properly in cells and were not retained by ER quality control machinery (Fig. 2D). The average T_1 (longitudinal) and T_2 (transverse) relaxation times (the ratio of which is proportional to the size of Ig^{MPZ}

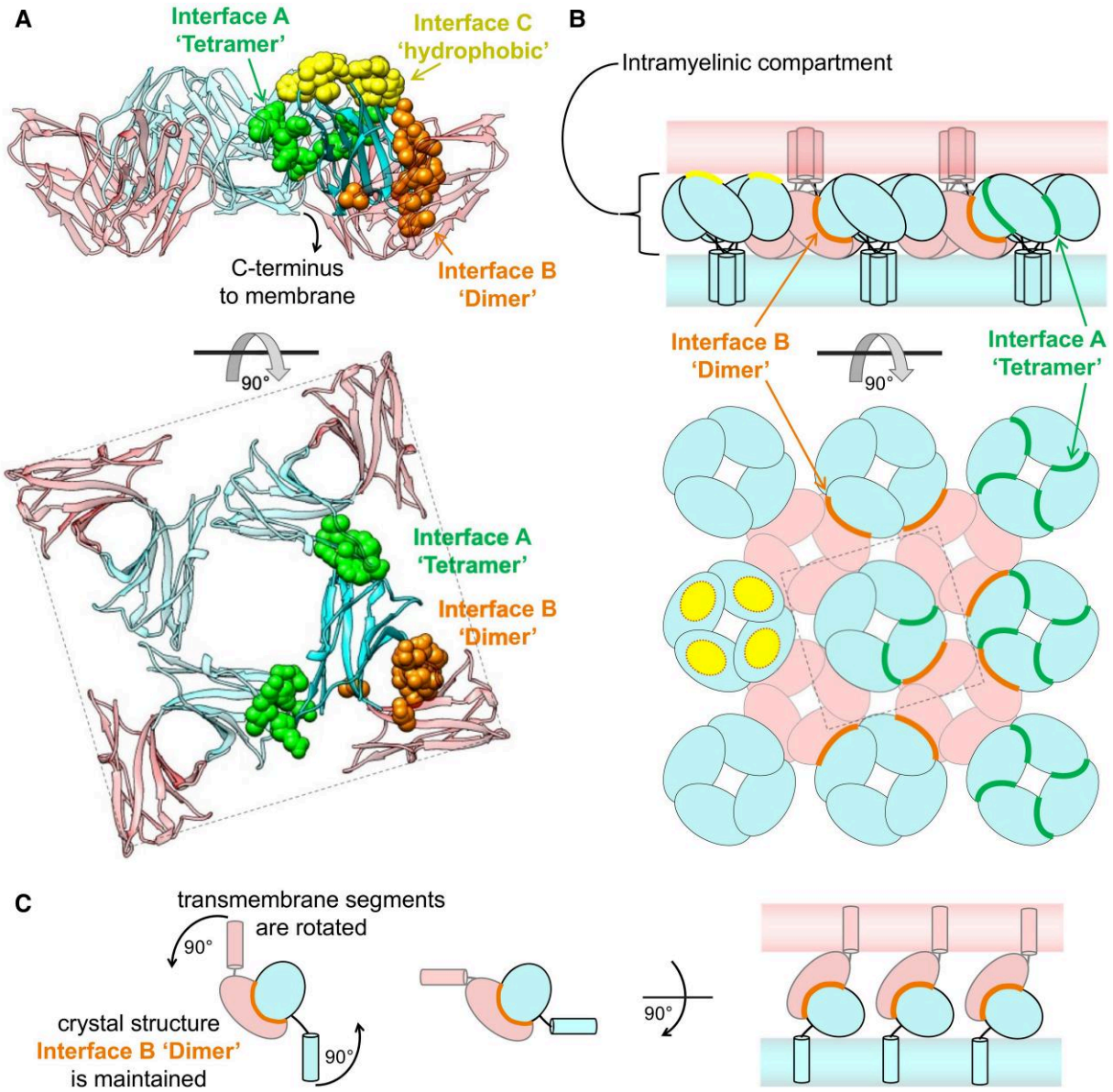

Figure 1 Current models for structural organization of Ig^{MPZ} functional assembly in myelin. (**A**) Intermolecular packing in the rat Ig^{MPZ} crystal structure (PDBid: 1NEU).[16] Ig^{MPZ} subunits organize into tetramers (cyan) with the C-terminus on the same side in a *cis* configuration. Each subunit in the tetramer is also dimerized to another Ig^{MPZ} subunit from an apposing membrane in a *trans* configuration (pink). Surface residues mediating the *cis*-tetramer (Interface A; green) and *trans*-dimer (Interface B; orange) interactions are displayed. Shown in yellow is another proposed interface (Interface C) made of hydrophobic residues that may associate directly with the lipid bilayer. (**B**) The oligomeric assembly model in **A**, schematized and extended in the context of the intraperiod line (*top*). Tetramers in one membrane, held together by the green tetramer Interface A, assemble with other tetramers of the apposing membrane via the orange dimer Interface B. (**C**) An alternate proposed model, lacking a tetramer Ig^{MPZ} where myelin wraps are held together by two apposing Ig^{MPZ} domains interacting through Interface B.

complexes) were measured over a range of Ig^{MPZ} concentrations (Fig. 2C). The T_1/T_2 data for wild-type Ig^{MPZ} showed a poor fit to monomer alone as predicted by HydroNMR,[29] and instead showed an increasing T_1/T_2 ratio with increasing protein concentrations indicating that oligomers assemble in the affinity range of ~100 μM. In contrast, both the $Ig^{MPZ}\Delta A$ and $Ig^{MPZ}\Delta A\Delta B$ mutants had a lower T_1/T_2 ratio across the same concentration range indicating that the extent of oligomerization was different from that of wild-type Ig^{MPZ}. However, the T_1/T_2 ratio of $Ig^{MPZ}\Delta A$ and $Ig^{MPZ}\Delta A\Delta B$ still increased in a concentration-dependent manner and were indistinguishable from one another, suggesting that oligomerization still occurred. One likely possibility was that there is more than one interface driving oligomerization and that the W53A mutation disrupted one of these (Interface A), but that the other interface was unaffected by mutating residues that mediate interaction through the hypothetical dimer interface (Interface B).

While T_1/T_2 data can differentiate between fully monomeric Ig^{MPZ} versus mixtures containing a proportion of Ig^{MPZ} oligomers, it lacks resolution above 25 kDa to differentiate between oligomer forms (e.g. dimers, tetramers). SAXS, a complementary solution-based method with increasing resolution at higher molecular weights, was used to discern the oligomeric status of wild-type Ig^{MPZ} (Fig. 3A, Supplementary Fig. 3 and Supplementary Table 3). Experimental SAXS curves generated from Ig^{MPZ} samples were fit

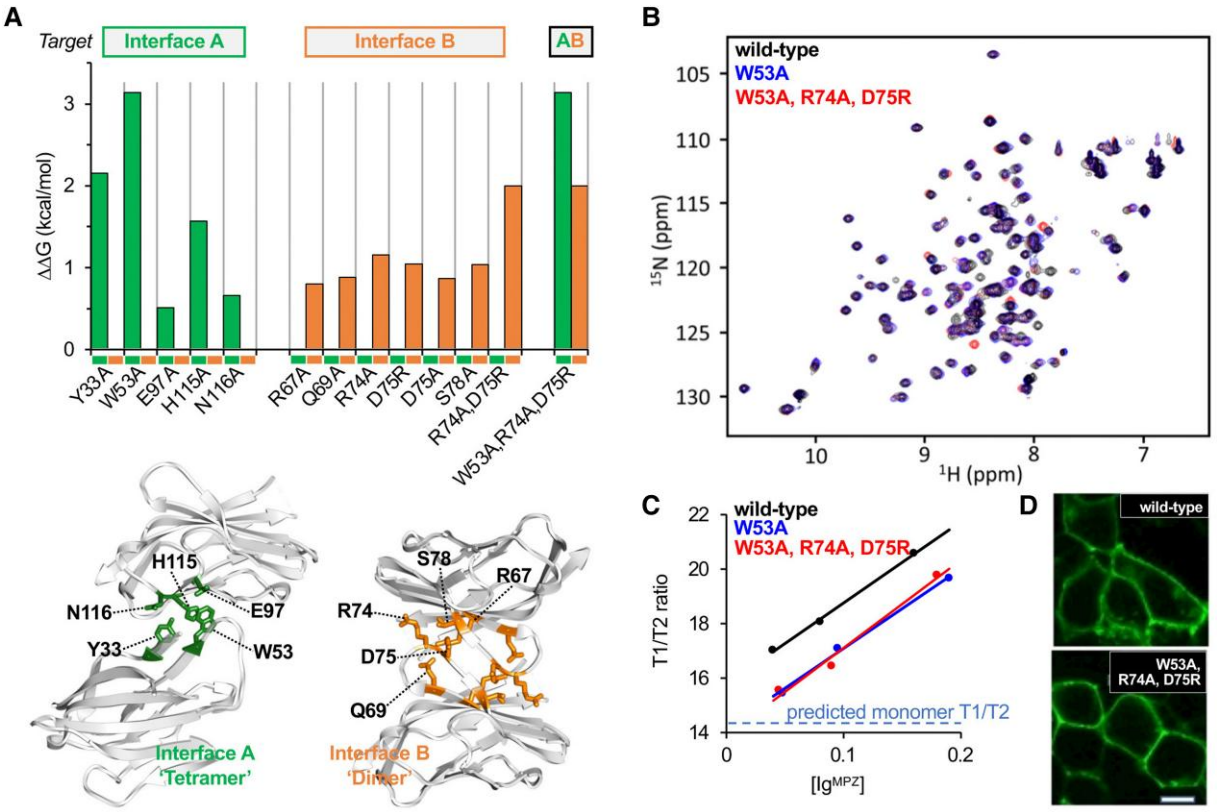

Figure 2 Engineered mutations targeting crystal structure dimer interface studied by solution nuclear magnetic resonance. Targeted mutagenesis coupled with nuclear magnetic resonance (NMR) analysis of Ig^{MPZ} confirms location of Interface A but not Interface B. (**A**) *Top*: To rationally design mutations that specifically disrupt protein interaction interfaces (bar labels above denote target), we used a computational approach to predict changes in binding energy for indicated amino acid substitutions within Ig^{MPZ} for the tetramer Interface A (green) and dimer Interface B (orange). Note that the W53A amino acid substitution mutant only has predicted effects on Interface A whereas the R74A, D75R double mutant only has predicted effects on Interface B. Data are graphed from calculations shown in Supplementary Table 2. *Bottom*: Structural diagrams of Ig^{MPZ} dimers bound via Interface A (*left*, green) or Interface B (*right*, orange). Interface mutants expected to cause the largest oligomeric disruptions were the top candidates to evaluate experimentally. (**B**) Overlay of $^{15}N/^{1}H$ HSQC NMR spectra of ^{15}N-labelled wild-type Ig^{MPZ} (black), the W53A mutant intended to disrupt the tetrameric Interface A (blue) Ig^{MPZ} ΔA, and the combined W53A, R74A, D75R triple mutant targeting both Interface A and the dimer Interface B (red) Ig^{MPZ} ΔAΔB. Most $^{15}N/^{1}H$ HSQC peaks of the three different proteins overlap showing that they share high degree of structural similarity and stability (individual spectrum displayed in Supplementary Fig. 2). (**C**) NMR analysis of molecular tumbling. The ratio of T_1 and T_2 relaxation times for ^{15}N-labelled wild-type Ig^{MPZ}, Ig^{MPZ} ΔA and Ig^{MPZ} ΔAΔB were measured and plotted as a function of protein concentration. An increase in T_1/T_2 ratio corresponds to an increase in molecular size related to oligomerization. For comparison, the predicted T_1/T_2 ratio of monomer only (blue hashed line) is also plotted. (**D**) Localization of C-terminally GFP-tagged wild-type MPZ (WT) or mutant MPZ ΔAΔB (W53A, R74A, D75R) expressed in HEK293 cells via transient transfection. MPZ ΔAΔB trafficked to the cell surface similar to wild-type MPZ showing both proteins were not retained in the endoplasmic reticulum (ER) and passed ER quality control.

to a mixture of curves computed from theoretical protein models of their predicted homo-oligomeric components. The proportions of each component curve were used to deduce the proportion of oligomers in the solution. The set of component oligomers in the fitting model were optimized to obtain computed SAXS curves with the best fits to empirical SAXS data. Using OLIGOMER,[43] our empirical SAXS data fit poorly to theoretical predictions containing only monomeric Ig^{MPZ} ($\chi^2 > 25$). In contrast, a theoretical curve generated from five oligomeric components had a very good fit ($\chi^2 = 0.99$). The minimal set of Ig^{MPZ} oligomers to obtain a reasonable fit ($\chi^2 < 1.5$) included monomer and tetramer. At higher concentration, equilibrium shifted away from monomers towards dimers, tetramers, 8-mers and 16-mers (Fig. 3C and Supplementary Table 4).

Because NMR data indicated that the Ig^{MPZ}ΔA mutant no longer formed tetramers, but that further mutation of the hypothetical dimer interface (ΔB) had no further effect on the ability to oligomerize (Fig. 2C), we also analysed the mutant Ig^{MPZ}ΔAΔB by SAXS (Fig. 3B). If both A and B interfaces operate, we would expect SAXS data to show a dramatic change fitting only Ig monomers, whereas if only the A interface operates without any effect of compromising the B interface, the Ig^{MPZ}ΔAΔB mutant would retain its ability to oligomerize but lack the ability to form tetramers. SAXS data showed that the Ig^{MPZ}ΔAΔB mutant still underwent concentration dependent oligomerization. However, the extent of Ig^{MPZ}ΔAΔB oligomerization was less than for wild-type Ig^{MPZ}, consistent with the NMR T_1/T_2 relaxation data, which also indicated less oligomerization. The fit of the Ig^{MPZ}ΔAΔB SAXS data to the theoretical oligomeric distributions optimized for wild-type Ig^{MPZ} showed that Ig^{MPZ}ΔAΔB still formed a dimer in a concentration-dependent manner, but had lost the ability to form tetramers and 8-mers (Fig. 3C and Supplementary Table 4).

These data substantiate that Ig^{MPZ} forms oligomers in solution and that at least two interfaces mediate these interactions. One of the interfaces relies on W53, supporting the idea that the tetrameric Interface A found in the crystal lattice of the rat Ig^{MPZ} indeed operates in solution. The data also suggest another interface that mediates Ig^{MPZ} dimerization, but one distinct from the dimer Interface B present in the rat Ig^{MPZ} crystal lattice (Figs 1A and 2A).

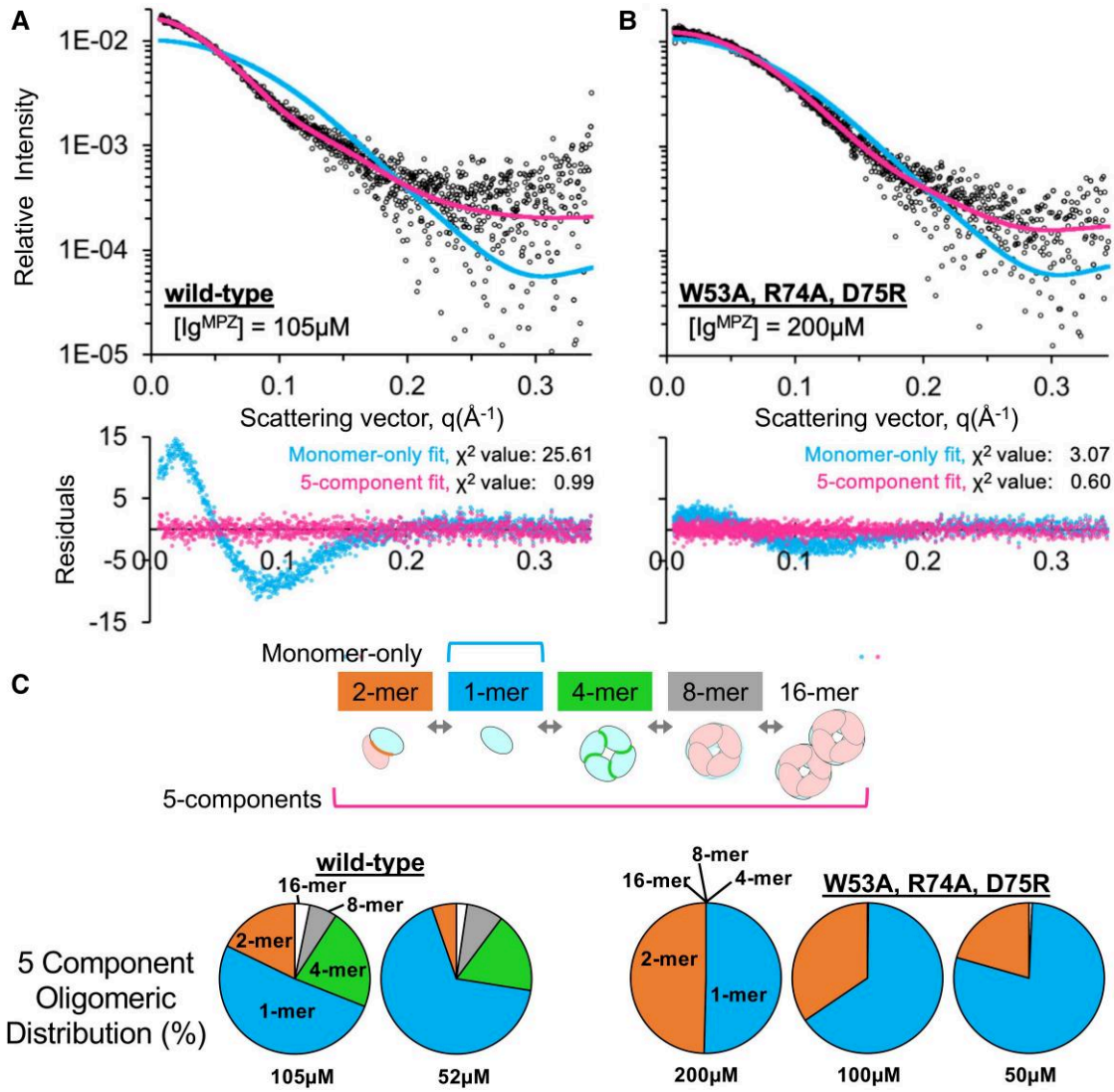

Figure 3 Human Ig^{MPZ} oligomer distribution in solution studied by small angle X-ray scattering. Small angle X-ray scattering (SAXS) data show that wild-type Ig^{MPZ} oligomerizes at μM concentrations forming monomers (blue), dimers (orange) and tetramers (green), whereas the Ig^{MPZ} ΔAΔB (W53A, R74A, D75R) mutant eliminated tetramer but not dimer formation. (**A**) *Top*: SAXS scattering data (circles) for 105 μM wild-type Ig^{MPZ}. Data are overlayed with the predicted curve for monomeric Ig^{MPZ} (blue) and a five-component fitted curve (pink). *Bottom*: Residuals of raw data against monomer only fit (blue) and five-component curve fit (pink) are shown along with calculated χ^2 values. (**B**) SAXS data (circles), monomer only fit (blue), five-component curve fit (pink) and residuals for Ig^{MPZ} ΔAΔB (W53A, R74A, D75R) measured at 200 μM. (**C**) Ig^{MPZ} oligomeric distributions obtained from five-component fits shown in **A** and **B** as well as diluted concentrations of 0.5× (both) and 0.25× (Ig^{MPZ} ΔAΔB). Curve fitting components (monomers, dimers, tetramers, dimeric-tetramers, dimeric-octamers) were modelled from the predicted oligomeric arrangement in the crystal structure (PDBid: 1NEU).[16] The proportions of each component that best fit experimental data are shown graphically (plotted from data in Supplementary Table 4).

Distribution of disease-causing variants in the Ig domain of MPZ reveals three subgroups

Our binding data demonstrated that the Ig^{MPZ} forms tetramers. Moreover, inspection of the transmembrane domain of MPZ shows that it contains two GxxxG motifs known to allow tight packing of transmembrane domains together.[44-46] These data support the idea that four MPZ proteins in the same membrane can form a tetramer (*cis*-tetramer) via their Ig domain. We next analysed the distribution of disease-causing patient amino acid substitution variants to determine whether there were any distinct subdomains of Ig^{MPZ} tetramers that correlate with different disease symptoms or mechanisms. Our intent was to determine if a predictive model for types of CMT could be generated based on structural correlates.

We also wanted to determine whether there were disease-related subregions on the Ig^{MPZ} surface that might serve as interaction sites, such as one that could constitute the unknown Ig^{MPZ} dimer interface. Two different forms of CMT can arise from variants in the Ig^{MPZ} domain.[47] One form, CMT2I/J, is characterized by axonal degeneration but with relatively normal myelin morphology and late-onset. The other form is demyelinating CMT1B, occurring earlier in life. Using patient variant data summarized in Supplementary Table 5, we calculated two parameters. One was the solvent-accessible surface area as a measure of how close the variants were located to the surface of the protein (Fig. 4A). The other parameter, calculated using DeepDDG,[41] predicted the effect of variants on the overall stability of the Ig^{MPZ} domain determined by the change in ΔG (Gibbs free energy change defining wild-type

protein stability) (Fig. 4B and Supplementary Table 5). We categorized patient variants as axonal late-onset CMT2I/J or demyelinating early-onset CMT1B. To reduce noise from variants lacking site-specific effects, we limited analysis to single amino acid substitutions, excluding deletions, frameshift or premature stop codon variants and we filtered out variants with significant variability in disease symptoms (S78L, R98H).[47] Variants previously identified as hyperglycosylating (D61N, D109N, D118N, K138N) were also excluded because the additional bulky surface sugar likely disrupts MPZ function in a distinct way.[48]

Overall, variants causing CMT2I/J were predicted to have far less of a destabilizing effect on the Ig^{MPZ} fold than the CMT1B group of variants ($P < 0.05$) (Fig. 4B). Likewise, the positions of the residues involved in CMT2I/J had a higher solvent accessible surface area indicating their position at the surface of the Ig^{MPZ} domain (Supplementary Fig. 4A), consistent with the lower propensity of surface residues in general to cause destabilization to a protein fold when mutated.[49] We refer to this set of residues as Group 1 (Table 1). Computationally predicting the effect of CMT1B variants on the stability of Ig^{MPZ} revealed two subgroups. One group had a low predicted effect on Ig^{MPZ} stability (non-destabilizing $CMT1B^{N}$, which we refer to as Group 2 residues). This group also had a high solvent accessible surface area (Supplementary Fig. 4B). Another separate group contained variants that were predicted to have large destabilizing effects on the Ig^{MPZ} fold (destabilizing $CMT1B^{D}$, which we refer to as Group 3 Ig^{MPZ} variant residues), had significantly lower levels of solvent accessible surface area (Table 1).

We next mapped the amino acid positions of the newly defined phenotype groups onto the modelled structure of a Ig^{MPZ} tetramer to discern if CMT disease phenotypes mapped to discrete subdomains (Fig. 4C). Residues that when mutated give rise to CMT2I/J (Group 1) largely map to a surface-exposed cluster of residues proximal to the MPZ transmembrane domain (Fig. 4C and Supplementary Fig. 4). This surface also surrounds the site where the *N*-linked glycan of ~3 kDa is attached. This sizable glycan would likely interact with this surface as well, possibly indicating that the critical nature of this subdomain is to properly engage or accommodate the *N*-linked glycan.

The location of variants causing CMT1B which are not predicted to destabilize the Ig^{MPZ} fold (Group 2, Table 1) largely mapped to a surface distal to Ig^{MPZ} tetramer transmembrane domains and closer to the apposing membrane (Fig. 4C). A 'top' view, looking at the tetramer from the apposing membrane, shows this surface is confined to the outer perimeter of the tetramer, ideally suited for interaction with other protein partners. This subregion is distinct from the hydrophobic region on the top of the Ig^{MPZ} domain nearest the apposing membrane that contains a patch of tryptophan residues previously proposed to associate with the apposing lipid bilayer and defined above as Interface C.[16]

The location of Group 3 variants, which were predicted to destabilize the Ig^{MPZ} fold (Table 1), largely map to the interior of each Ig^{MPZ} domain (Fig. 4C), consistent with the idea that the amino acids critical to the integrity of the Ig^{MPZ} fold would be located within the core of the protein farther from the surface.[49]

Different spatial distribution groups correlate with disease mechanism

One of the best understood pathogenesis pathways for how MPZ mutations causes autosomal-dominant CMT is by provoking the UPR and promoting ER stress.[23,50] This occurs when improperly folded MPZ accumulates in the ER, triggering signalling through PERK, IRE1 and ATF6.[51] Previous studies in cultured cells have surveyed various patient variants throughout the Ig^{MPZ} domain for their propensity to accumulate in the ER and to elicit UPR.[25] However, not all CMT1B-causing variants evoke UPR implying that there are additional mechanisms that can drive demyelinating CMT. The analysis in Fig. 4 differentiated a group of CMT1B variants that were predicted to destabilize the Ig^{MPZ} domain from a group of variants with low predicted effect on the Ig^{MPZ} stability. Therefore, we tested whether these computed effects correlated with how these variants evoked the UPR, as described in previous studies.[25] To generate a numerical index, we combined values that measured UPR transcriptional response as well as the degree of ER localization (Supplementary Table 6). We found the destabilizing group of CMT1B variants that largely map to residues in the core of the Ig^{MPZ} (Group 3, $CMT1B^{D}$) evoked the UPR significantly ($P < 0.05$) more than the non-destabilizing group of CMT1B variants (Group 2, $CMT1B^{N}$) that largely map to surface-exposed residues (Fig. 5). These data suggest not only a way to predict which Ig^{MPZ} variants would trigger a pathogenesis pathway driven by ER stress, but suggests that disrupting the function of a different part of the Ig^{MPZ}, namely the surface on the distal exterior of Ig^{MPZ} tetramers (Fig. 4), fulfils a distinct function that when compromised leads to a different disease mechanism that drives CMT1B.

Potential involvement of disease-relevant surface subregions of Ig^{MPZ} in dimerization

Two of the three variant position groups (Group 1: CMT2I/J and Group 2: $CMT1B^{N}$) defined subregions on the surface of Ig^{MPZ} tetramers having the potential to mediate specific biomolecular interactions. Because our NMR and SAXS analysis demonstrated that Ig^{MPZ} dimerizes but that the identity of the dimerization interface remains undefined, we used computational docking methods to find whether a particular subregion on the Ig^{MPZ} surface was favoured for dimerization. Using ClusPro,[42] we found 71 clusters of dimer poses using one Ig^{MPZ} monomer binding to another Ig^{MPZ} monomer (Fig. 6A) using four scoring schemes that differed in how they weigh energy coefficients (e.g. favouring electrostatic, hydrophobic or van der Waals forces). Poses were filtered to find those that did not produce steric clashes in the context of Ig^{MPZ} tetramers (Fig. 6A). This produced only five tetramer-compatible poses (Fig. 6D) in addition to the dimer interface extrapolated from the 1NEU crystal structure (Fig. 6C). The five new poses were identified with a scoring scheme that favoured a mix of electrostatic interactions combined with van der Waals (shape complementarity). Strikingly, these interfaces involved surface residues from the group (Group 2: $CMT1B^{N}$) of surface-exposed non-destabilizing CMT1B variants located on the outer distal surface of the Ig^{MPZ} tetramer (Fig. 4C and Table 1). To view this quantitively, we calculated the average distance for the 10 CMT1B (Group 2) residues to the docked Ig^{MPZ} surface for each dimer pose as well as the same parameter for the 12 CMT2I/J (Group 1) residues (Fig. 6B and Supplementary Fig. 5). These values showed that the Ig^{MPZ} dimerization interfaces were closer to the $CMT1B^{N}$ surface (Group 2 residues) than to the CMT2I/J surface (Group 1 residues) (Fig. 6B and Supplementary Fig. 6). Only one pose (6_9 in Fig. 6) docked onto the tetramer such that it was closer to the Group 1 'CMT2I/J' surface. However, this pose places two tetramers at an angle that is incompatible with the insertion of the transmembrane domains within either the same membrane or apposing membrane lipid bilayer across the intraperiod line (Fig. 6D, lower). Comparing the surface regions defining the interfaces used by the remaining

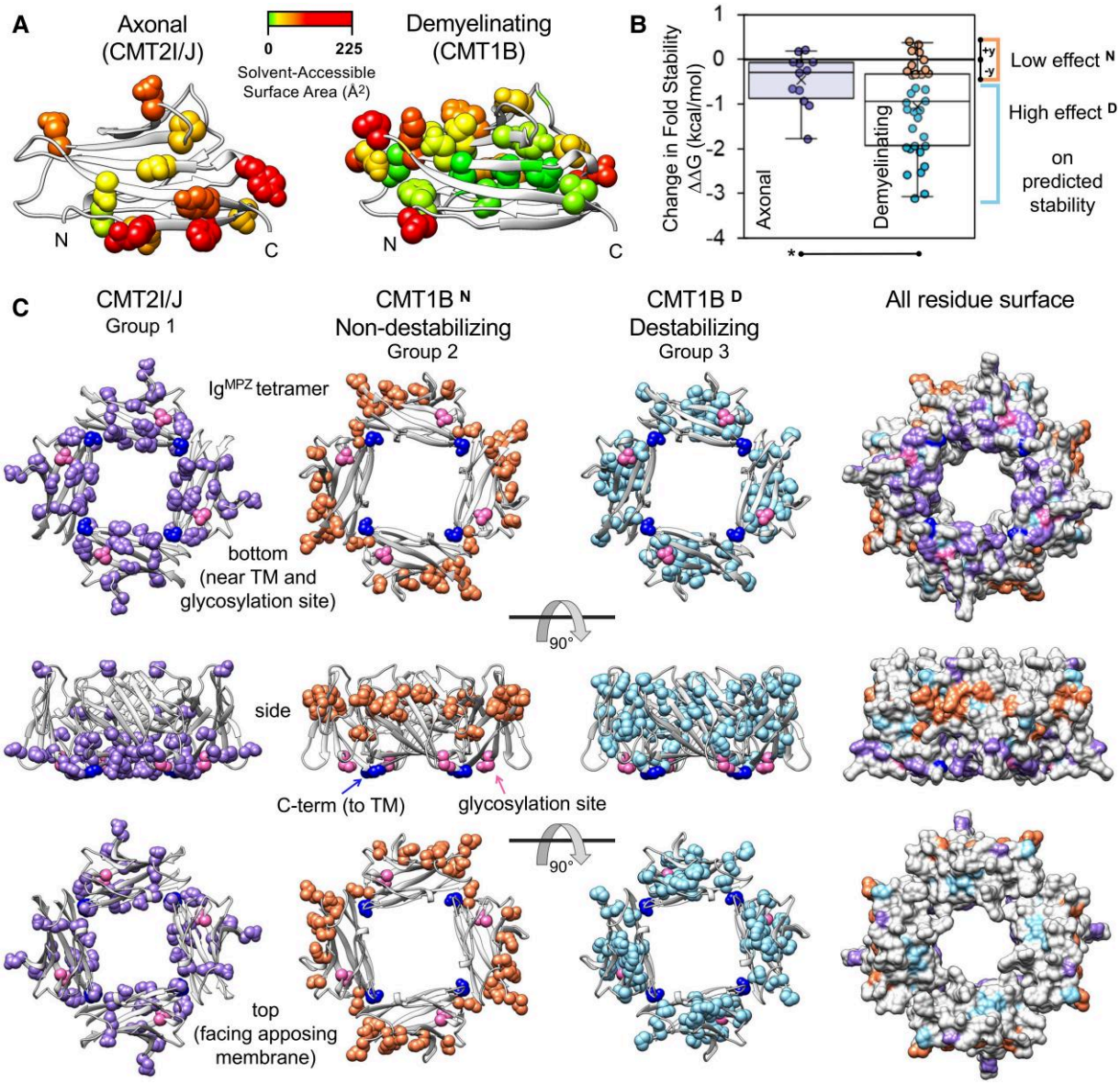

Figure 4 Structurally distinct regions of Ig^{MPZ} tetramers correlate to disease phenotypes. (**A**) Surface accessibility of wild-type Ig^{MPZ} residues with amino acid variants that cause axonal CMT2I/J or demyelinating CMT1B. Positions were mapped onto the human Ig^{MPZ} structure (PDBid: 3OAI)[17] and colour-coded for solvent-accessible surface area. A larger percentage of CMT1B linked residue positions are buried. (**B**) Patient variants causing different CMT types defined previously[47] (axonal CMT2I/J or demyelinating CMT1B and listed in Supplementary Table 5) were computationally evaluated for whether they would destabilize the Ig^{MPZ} structure quantified as a change in predicted ΔG for Ig^{MPZ} stability. Demyelinating CMT1B patient variants had on average a higher prediction for destabilization than axonal CMT2I/J linked variants (*$P < 0.05$). The CMT1B patient variants could be divided into two subgroups: one with low predicted effects on stability (^{N}), and another with high predicted effects on stability (^{D}). (**C**) The three groups of residue positions (Table 1) are shown in the context of the Ig^{MPZ} tetramer in three viewing orientations. Group 1 (violet) are residues mutated in CMT2I/J; Group 2 (orange: $CMT1B^N$) are residues mutated in CMT1B that result in low predicted effects on Ig^{MPZ} stability; and Group 3 (light blue: $CMT1B^D$) showing positions of CMT1B mutations predicted to destabilize the Ig^{MPZ} domain. *Right*: Using the molecular surface of the tetramer, coloured patches indicate the solvent accessible residues in the context of surrounding residues. A CMT2I/J patch is visible on the bottom surface of the Ig^{MPZ} tetramers near the transmembrane domain and glycosylation site, while a $CMT1B^N$ patch is visible along the side view. Surface-inaccessible (buried) residues are not visible in this schematic. Supplementary Fig. 4 shows that the $CMT1B^D$ (Group 3) residues have significantly lower levels of surface accessibility than other residue groups.

Table 1 Residue position groups defined by CMT type and biophysical parameters

Group 1: Residues wherein variants cause axonal CMT2I/J	Group 2: $CMT1B^N$ Residues wherein variants cause demyelinating CMT1B but NOT predicted to destabilize Ig^{MPZ}	Group 3: $CMT1B^D$ Residues wherein variants cause demyelinating CMT1B and predicted to destabilize Ig^{MPZ}
D35, R36, H39, S44, S51, D61, P70, D75, Y119, T124, S140, Y145	I30, S63[a], H81, D90, N116, D128, K130, D134, I135, G137	F52, T65, Y68, Y82, G93, R98, W101, G103, G110, S111, I112, I114, G123, C127, N131, P133, V146

[a]Average predicted stability for S63 is in Group 2; includes S63F (Group 2) and S63C (Group 3, near cut-off).

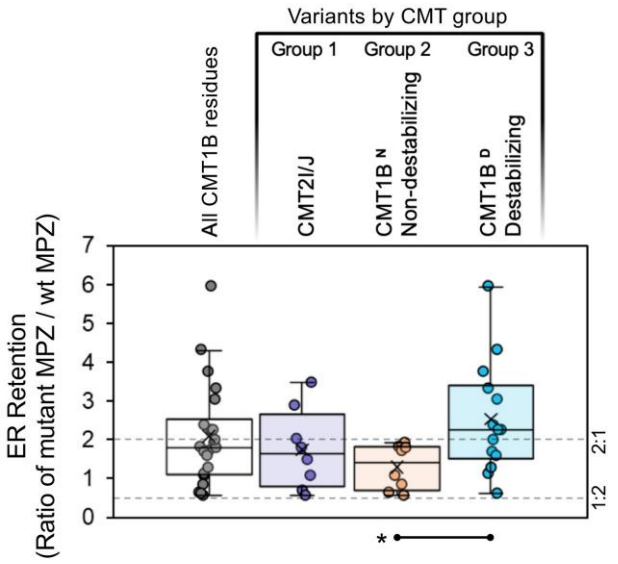

Figure 5 Endoplasmic reticulum retention of MPZ as a function of CMT Ig^{MPZ} variant groups. The ability of different CMT-causing MPZ amino acid variants to promote endoplasmic reticulum (ER) retention and activate the unfolded protein response (UPR) was previously determined.[25] For each CMT Ig^{MPZ} variant, measurements were averaged and grouped for CMT2I/J (Group 1), and the two CMT1B subgroups (Groups 2 and 3). $CMT1B^{N}$ (Group 2) and $CMT1B^{D}$ (Group 3) were classified as described in Fig. 4B and listed in Table 1. The average ER retention and activation of UPR for non-destabilizing and destabilizing CMT1B variant subgroups is significantly different. (*$P < 0.05$). For variants that did not cause ER retention and UPR had an index in the range between ratio between 2:1 and 1:2 and 2:1 whereas variants that had dramatic ER retention and UPR exceeded 2:1. Data plotted for this evaluation are listed in Supplementary Table 6.

computational dimer poses with the surface regions containing CMT2I/J variants and $CMT1B^{N}$ variants shows good overlap with the latter but not the former (Supplementary Fig. 7). We also used these models to fit SAXS data generated with the $Ig^{MPZ}\Delta A\Delta B$ domain, which formed only monomers and dimers to determine if any of these models was favoured. While including model 6_14 as the dimer had the best fit (χ^2 0.599, Rg 20.67), it was comparable to that given by Interface B (χ^2 0.599, Rg 21.48) and only slightly better than other models. Importantly, fits using dimers modelled through Interface A (χ^2 0.712, Rg 23.06) or Interface C (χ^2 1.250, Rg 27.12) were much worse, supporting the conclusion that these latter interfaces are not used for dimer formation but that the computational dimer models are plausible. Overall, the observation that the computational predictions for dimer formation are compatible within the context of linking tetramers and map to surface residues relevant to CMT1B suggests that this surface patch could be disease-relevant by mediating tetramer-tetramer interactions.

Discussion

MPZ is the major membrane protein expressed in Schwann cells and mediates myelin formation. The adhesion activity of MPZ is observed in heterologous cultured cells when ectopically expressed[11,12] and MPZ knockout mice have poorly compacted myelin sheaths.[13] It is thought that MPZ oligomerizes across the intraperiod line of myelin to hold apposing wraps of Schwann cell plasma membranes together, thus providing a key structural role in forming myelin. Mutations throughout MPZ as well as just the Ig^{MPZ} domain cause autosomal dominant CMT disease, a collection of hereditary motor and sensory neuropathies,[21,47,52-54] that are characterized either by poorly formed myelin (CMT1B) or by axonal degeneration wherein the structure of myelin is relatively intact (CMT2I/J). These facts pose several distinct unanswered questions about how the Ig^{MPZ} domain operates in both normal myelinating Schwann cells and in disease pathogenesis. Key to addressing these questions is to understand the structural basis of Ig^{MPZ} oligomerization, its role in normal myelination and whether perturbation of oligomerization might drive autosomal dominant CMT2I/J or CMT1B.

Current models propose that adhesion of myelin wraps is mediated by Ig^{MPZ} oligomerization itself, however this has not been tested.[16,18,20] Our data suggest that Ig^{MPZ} has two distinct oligomerization modes. One of those is predicted from crystal packing of the rat Ig^{MPZ} domain and works by bundling four MPZ proteins anchored in the same membrane together, forming a *cis*-tetramer (Fig. 1B). Our SAXS data support the model whereby Ig^{MPZ} tetramerizes in the ~100 μM range through an interface that relies on W53 interactions, consistent with the arrangement of tetramers via crystal packing in the rat Ig^{MPZ} crystal structure. While W53A-mutant Ig^{MPZ} domains do not form tetramers, they still dimerize. The current models for how MPZ mediates adhesion across the intraperiod line relies on a *trans* interaction of MPZ proteins from each apposing membrane. Mutating the hypothetical dimer Interface B extrapolated from crystal packing, which is postulated to mediate this *trans* configuration, did not diminish dimerization. Thus, interface B is unable to explain how MPZ is linked across the intraperiod line making alternative models distinct possibilities (Fig. 7).

Recently, Raasakka and Kursula proposed an alternate model (Fig. 1C) for how Ig^{MPZ} could mediate adhesion of myelin wraps via zippering of *trans* dimers.[18,20] That model proposes that the dimer interface is Interface B but is working at a more oblique angle than positioned in the model of Shapiro.[16] Our data support the idea of dimer formation, but not through Interface B, and alternative dimer interfaces could not be resolved with the low resolution cryo-EM images Rassakka *et al.*[18] used to formulate the zipper model. Certainly, other *trans* dimer configurations are possible (e.g. model 6_18, Fig. 6); however, the more substantial discrepancy between our results and the model of Rassakka *et al.*[18] is the omission for a role of Ig^{MPZ} tetramers, which clearly form in solution. It is possible that tetramers might not form in the context of full-length MPZ in biological membranes. Such a conformation requires the transmembrane domains (TMD) of MPZ protomers to come together in close contact, essentially bundling like stems in a flower bouquet of Ig^{MPZ} domains. Notably, the membrane-spanning segment of MPZ has two GxxxG motifs that have been found to allow for close packing of transmembrane domains, bolstering the plausibility that full-length MPZ might form *cis* tetramers.[44-46] Another feature of MPZ is its *N*-linked glycosylation, occurring on an Asn residue within a region of the Ig^{MPZ} domain near the membrane that it is inserted into, which would not be predicted to interfere with tetramer formation (Fig. 4C). Moreover, previous X-ray scattering data from SDS-solubilized full-length MPZ were compatible with tetrameric MPZ complexes.[55] Thus, in our view, the possibility that MPZ forms tetramers in native myelin membranes is plausible.

One of the central features of the model from Shapiro *et al.*[16] is that Interface B nicely mediates an Ig-Ig interaction between two myelin wraps that fits within the ~45 nm of the intraperiod line of compacted myelin. Our data showing that Interface B does not

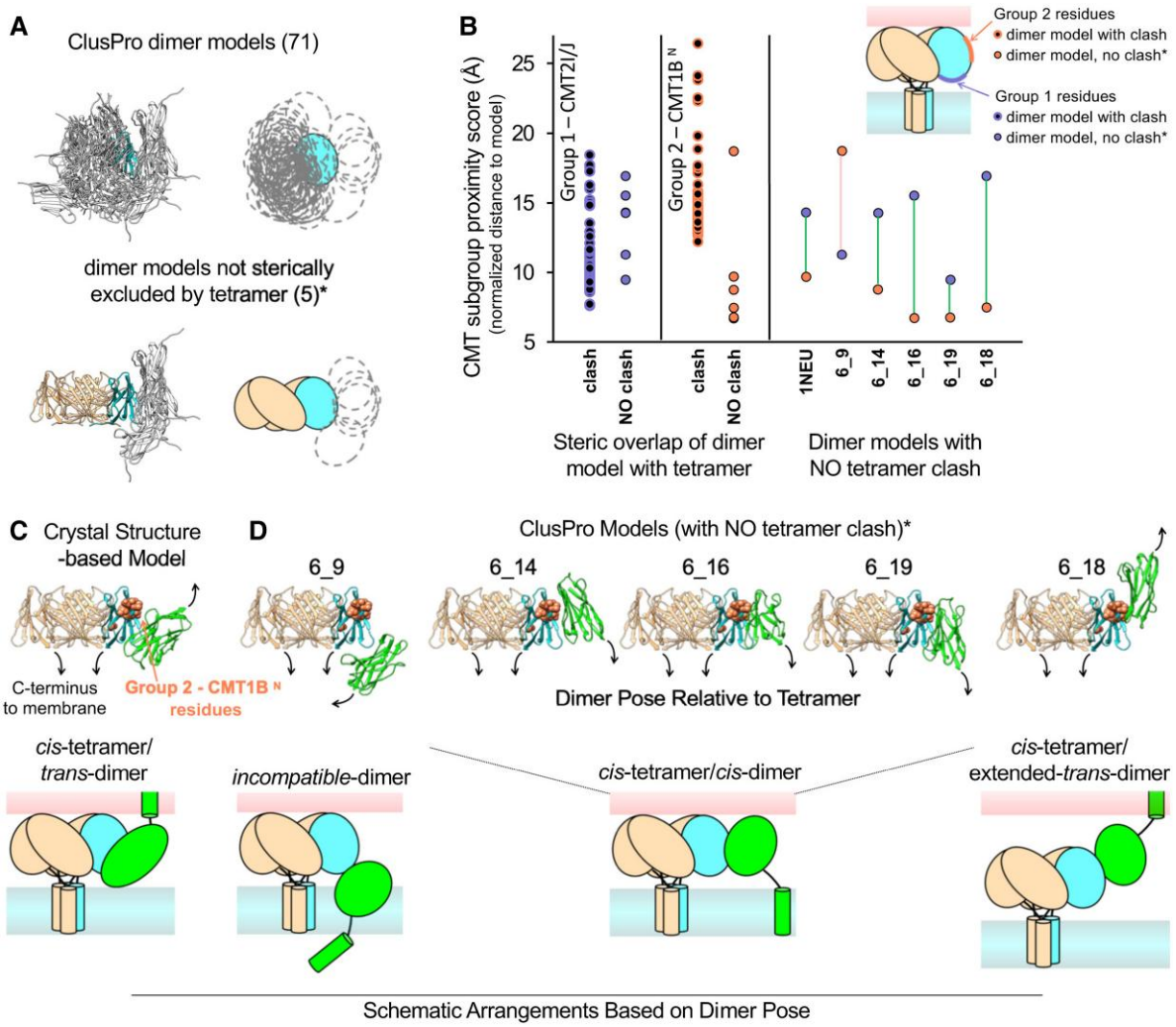

Figure 6 Evaluation of Ig^{MPZ} dimer docking models for tetramer compatibility and proximity to CMT subgroup residues. Computational docking experiments reveal that the $CMT1B^N$ (Group 2) surface subregion may mediate how a *cis*-Ig^{MPZ} tetramer binds (dimerizes) to another tetramer. (**A**) Dimer docking poses between Ig^{MPZ} monomers calculated using ClusPro (*top*) were filtered for those that were sterically compatible in the context of Ig^{MPZ} tetramers. Five of 71 dimer arrangements (*bottom*) could be positioned without overlapping a coexistent tetramer. (**B**) ClusPro models that had no clash in the context of Ig^{MPZ} tetramers or that were excluded because of clash were evaluated for their proximity to CMT2I/J (Group 1) and $CMT1B^N$ (Group 2) linked residues. For each model, a subgroup proximity score was calculated by summing the shortest distance between each subgroup residue and the docked Ig^{MPZ} for the dimer model being evaluated and normalized by the total subgroup residues. *Right*: For each of the tetramer compatible dimer models, the subgroup proximity score for CMT2I/J (Group 1) (violet) and $CMT1B^N$ (Group 2) (orange) variants were directly compared. (**C**) *Top row*: Cartoon ribbon model for an Ig^{MPZ} monomer (cyan) with coexistent homo-tetramer (orange) and *trans* homo-dimer (green) subunits positioned according to Ig^{MPZ} packing in the rat crystal structure (PDBid: 1NEU).[16] $CMT1B^N$ (Group 2) variant linked residues (orange) are displayed on the cyan Ig^{MPZ} subunit. *Bottom row*: Depiction of predicted arrangement across the intraperiod line of a *trans* homo-dimer interacting (green) subunit. (**D**) Five alternative ClusPro Ig^{MPZ} dimer docking poses (for incompatible-, *cis*- and extended-*trans*-) identified in **A** with the same model depictions and colour schemes as **C**.

operate in solution illustrates the need to re-evaluate how MPZ oligomerization could fulfil its adhesion function (Fig. 7). Computational models produced two possibilities. One is that a dimer interface would link multiple MPZ tetramers all within the same membrane, promoting the formation of a large hydrophobic tryptophan-containing surface on the distal top of MPZ clusters. Such clusters of MPZ may correspond to the intramembrane particles that emanate from each myelin wrap observed in freeze fracture electron microscopy studies, as previously hypothesized.[56] Another possibility is that the dimer interface could work in trans across the intraperiod line, but in a way that does not operate in compact myelin. The 6_18 pose (Fig. 6) has a '*trans*' orientation, but is extended and would bridge a much larger gap between membranes than is observed in the intraperiod line of compacted myelin. Such an extended configuration could act as an intermediate step, holding the intraperiod line together but with larger spacing until an additional process compresses membrane apposition (Fig. 7). Interestingly, an S63C mutation, located with the $CMT1B^N$ surface subregion, appears to cause a disulphide linkage between Ig^{MPZ} domains resulting in a wider 70 Å intraperiod line that can be compressed when the disulphide linkage is reduced, implying the interface that is locked by a disulphide bond may represent one that is used naturally yet transiently during myelin formation.[57] Future efforts to assess the physiological consequences of MPZ mutants that lack specific oligomeric interfaces, such as the W53A mutation that blocks tetramer formation, will be helpful to resolve how this biochemical property plays a role for normal myelin development and how perturbation of these properties

may play a role in CMT. Breaking these interfaces may work to cause dominant CMT1B as our structural and genetic studies suggest. Alternatively, loss of oligomerization might be recessive, resulting in haploinsufficiency that results in the type of demyelinating and later onset CMT disease observed in heterozygous MPZ$^{-/+}$ mice[58,59] and in partial loss of MPZ function in patients.[60]

We also investigated whether there might be functionally distinct regions of an Ig^{MPZ} tetramer that correlate with different disease symptoms and mechanisms. By computationally calculating which patient missense variants are likely to destabilize the integrity of the Ig^{MPZ} fold, we defined three discrete subregions of Ig^{MPZ} with differing molecular pathologies. Variants causing demyelinating CMT1B generally map to two regions. One region was within the core of the Ig^{MPZ} where variants were predicted to have a destabilizing effect on the integrity of the Ig^{MPZ} fold (Group 3: CMT1B^{D}). The localization of these variants to the Ig^{MPZ} core correlated with their ability to activate the UPR when expressed in heterologous cells. A different group of CMT1B variants mapped to a surface lining the exterior distal surface of Ig^{MPZ} tetramers where they pose little danger of destabilizing the Ig domain but are ideally suited for mediating protein:protein interactions (Group 2: CMT1B^{N}). This observation suggests the existence of two distinct CMT1B disease mechanisms, one being where misfolded MPZ causes the dominant, deleterious activation of ER stress and another where alteration of the Ig^{MPZ} perturbs a functional interaction on the tetramer surface. Interestingly, another class of variants that cause gain of N-linked glycosylation has been found that do not cause ER stress and may also work like Group 2 variants to sterically perturb Ig^{MPZ} protein interactions.[48] Having structurally defined groups of variants that correspond to different disease mechanisms would help explain why UPR activation does not correlate with all CMT1B variants or CMT1B severity.[25] These distinctions will be important in the future to ensure treatments are matched to the correct CMT disease mechanisms. Recently an inhibitor (IFB-088, Sephin1) of the GADD34/PPP1R15A phosphatase complex, which works to potentiate the integrated stress response, has been used to successfully treat mice with CMT1B variants (S63del and R98C) that trigger the UPR and is entering phase 2 trials.[50,61] As a single amino acid substitution mutant, the R98C mutant falls clearly within Group 3 of destabilizing variants (Table 1 and Supplementary Table 5). We suggest the efficacy of Sephin1 treatment may correlate best for the Group 3 CMT1B^{D} destabilizing variants versus CMT1B^{N} variants that map to the Ig^{MPZ} surface. We note that not all CMT1B^{D} variants strongly evoke the UPR and are retained in the ER. Outliers such as T65N, Y82C, P133A have large predicted effects on the stability of the Ig fold, but cause low levels of ER retention and UPR. It is not precisely known what the ER quality control machinery recognizes about its protein clientele.[62] Thus, these changes might disrupt the fold in substantial ways to alter its function, but not trigger the dramatic ER retention that other disruptions do. Understanding these outliers (Supplementary Figs 8 and 9) will be important to assess efficacy of Sephin1 clinical trials.

The function of the Group 2 'CMT1B^{N} surface' remains to be determined, but it is optimally positioned to mediate protein-protein interaction with an Ig^{MPZ} tetramer. Our computational experiments found that alternate modes of Ig^{MPZ} dimerization involved this surface supporting the idea that this region could play a key role in oligomerization and partly explains how perturbation of this surface might contribute to demyelinating disease. Nonetheless, it is less clear whether or how loss of an Ig^{MPZ} oligomerization interface might drive autosomal dominant CMT disease. Inability of half of the Ig^{MPZ} domains to mediate critical oligomerization events could disrupt the regularity of larger MPZ assemblies that ultimately adhere myelin wraps together, or alter the ability of MPZ to signal to cytosolic components to drive compaction of the major dense line.[12,63]

Spatial mapping also revealed that residues involved in axonal CMT2I/J were on the bottom proximal surface of the Ig^{MPZ} tetramer (Group 1). Moreover, patient variants that give rise to CMT2I/J were

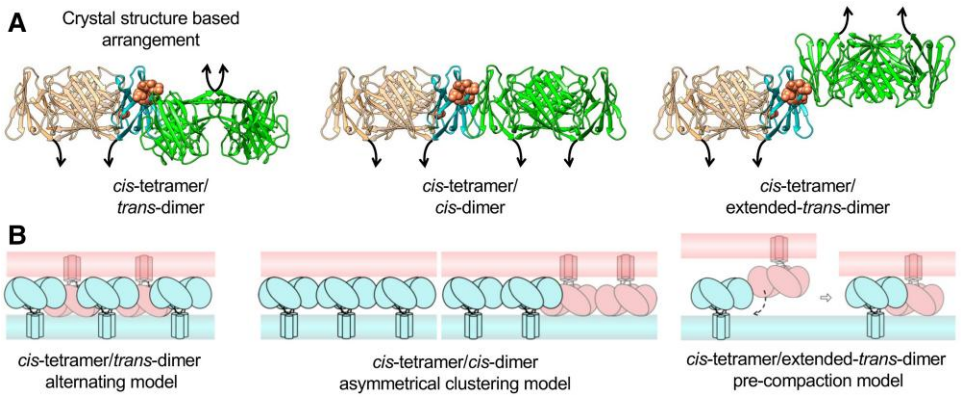

Figure 7 Possible tetramer-tetramer arrangements across intraperiod line. (**A**) Configurations of neighbouring Ig^{MPZ} homo-tetramers with steric viability across the intraperiod line. *Left* shows configuration based on the packing arrangement in the rat Ig^{MPZ} crystal structure (PDBid: 1NEU). *Middle* shows alternate configuration of interacting tetramers, where both Ig^{MPZ} homo-tetramers are anchored in the same membrane, is based on the 6_16 ClusPro model in Fig. 6D. Models 6_14 and 6_19 suggest similar *cis* tetramer-tetramer interaction surfaces. *Right* shows the 6_18 pose with the two Ig^{MPZ} tetramers linked in a *trans* configuration across in an extended arrangement that is accommodated with a larger distance between apposing membranes. The colour scheme is the same as in Fig. 6. (**B**) Hypothetical schematic arrangements of MPZ within myelin and potential roles of CMT1B^{N} (Group 2) variant linked residues. *Far left*: The model developed by Shapiro *et al.*[16] is based on the Ig^{MPZ} crystal contacts.[16] *Middle* shows arrangements whereby multiple MPZ tetramers are held together in *cis* via a dimer interface. This could allow MPZ to form clusters within the plasma membrane to make areas of local asymmetry rather than a strictly interdigitated arrangement as hypothesized from the crystal structure-based arrangement. *Far right* shows the homo-dimer interaction in the 6_18 ClusPro pose. Tetramer-tetramer interaction would span ~70 Å, which is wider than the ~45 Å span between membrane bilayers across the intraperiod line in compacted myelin. This extended *trans* conformation could serve a transition step during the initial assembly of myelin wraps, to be later reconfigured during myelin compaction.

not computationally predicted to compromise the stability of the Ig^{MPZ} fold, even though some of these variants can evoke the UPR indicating that they do not efficiently pass through the ER quality control system (Supplementary Figs 8 and 9). One key difference is that while computational studies consider only the Ig^{MPZ} protein, when expressed in cells, the Ig^{MPZ} domain also undergoes *N*-linked glycosylation. Moreover, the 'CMT2I/J -surface' surrounds the glycosylation site suggesting this region likely interacts with the glycan in a particular way, perhaps to properly position the Ig^{MPZ} domain with respect to the membrane. Indeed, mutations in the consensus *N*-linked glycosylation site ($N_{122}XT$) cause late-onset CMT2I/J in humans and mice[54,64] with morphological changes in the areas of non-compacted myelin and paranodes that communicate with underlying axons. Glycosylation has also been found to alter the adhesion activity of MPZ in heterologous systems, suggesting it helps optimally position Ig^{MPZ} for interactions.[65,66] We suggest that the effect of the Group 1 CMT2I/J variants is to affect the interaction with the glycan and in so doing mimic the effect that loss of the glycan altogether has on myelin function. Going forward, the key to understanding how variants within he CMT2I/J region cause disease could be a detailed characterization of the molecular and cellular defects of the T124M MPZ mutant that lacks *N*-linked glycosylation.

Data availability

The SAXS experimental data, oligomer fittings, and models from this study are deposited in SASBDB with accession codes: SASDRC3 (Ig^{MPZ}), SASDRD3 ($Ig^{MPZ}\Delta A\Delta B$). https://www.sasbdb.org/data/SASDRC3, https://www.sasbdb.org/data/SASDRD3. A project summary can be found here: https://www.sasbdb.org/project/1973.

Acknowledgements

We thank Dr Tom Rutkowski (U. Iowa) for helpful discussions and functional insights. We acknowledge the University of Iowa personnel and instrumentation in the IIHG Genomic Sequencing, the Carver College of Medicine NMR, and Protein and Crystallography core facilities, supported by the Roy J. and Lucille A. Carver College of Medicine and grants from the Roy J. Carver Charitable Trust. We acknowledge Sankar Baruah, Gretchen Stennett, and Tabitha Verhage for help with protein purification, Srinivas Chakravarthy, and Maxwell Watkins for help collecting SAXS data, and Manuela Ayee for helpful discussions.

Funding

This research used resources of the Advanced Photon Source, a U.S. Department of Energy (DOE) Office of Science User Facility operated for the DOE Office of Science by Argonne National Laboratory under Contract No. DE-AC02-06CH11357. BioCAT was supported by grant P30 GM138395 from the National Institute of General Medical Sciences of the National Institutes of Health. The content is solely the responsibility of the authors and does not necessarily reflect the official views of the National Institute of General Medical Sciences or the National Institutes of Health. This work was supported by NIH-R01 GM106568 to C.A.A., U54NS065712 to M.E.S., and NIH RO1GM058202 to R.C.P. C.A.A. and R.C.P. were supported by the Roy J. Carver Charitable Trust.

Competing interests

The authors report no competing interests.

Supplementary material

Supplementary material is available at *Brain* online.

References

1. Skre H. Genetic and clinical aspects of Charcot-Marie-Tooth's disease. *Clin Genet*. 1974;6:98-118.
2. Fridman V, Bundy B, Reilly MM, *et al*. CMT Subtypes and disease burden in patients enrolled in the Inherited Neuropathies Consortium natural history study: A cross-sectional analysis. *J Neurol Neurosurg Psychiatry*. 2015;86:873-878.
3. Murphy SM, Laura M, Fawcett K, *et al*. Charcot-Marie-Tooth disease: Frequency of genetic subtypes and guidelines for genetic testing. *J Neurol Neurosurg Psychiatry*. 2012;83:706-710.
4. Hayasaka K, Himoro M, Sato W, *et al*. Charcot-Marie-Tooth neuropathy type 1B is associated with mutations of the myelin P0 gene. *Nat Genet*. 1993;5:31-34.
5. Eylar EH, Uyemura K, Brostoff SW, Kitamura K, Ishaque A, Greenfield S. Proposed nomenclature for PNS myelin proteins. *Neurochem Res*. 1979;4:289-293.
6. Greenfield S, Brostoff S, Eylar EH, Morell P. Protein composition of myelin of the peripheral nervous system. *J Neurochem*. 1973;20:1207-1216.
7. Lemke G, Axel R. Isolation and sequence of a cDNA encoding the major structural protein of peripheral myelin. *Cell*. 1985;40:501-508.
8. Uyemura K, Asou H, Takeda Y. Structure and function of peripheral nerve myelin proteins. *Prog Brain Res*. 1995;105:311-318.
9. D'Urso D, Brophy PJ, Staugaitis SM, *et al*. Protein zero of peripheral nerve myelin: Biosynthesis, membrane insertion, and evidence for homotypic interaction. *Neuron*. 1990;4:449-460.
10. Eichberg J, Iyer S. Phosphorylation of myelin protein: Recent advances. *Neurochem Res*. 1996;21:527-535.
11. Filbin MT, Walsh FS, Trapp BD, Pizzey JA, Tennekoon GI. Role of myelin P0 protein as a homophilic adhesion molecule. *Nature*. 1990;344:871-872.
12. Xu W, Shy M, Kamholz J, *et al*. Mutations in the cytoplasmic domain of P0 reveal a role for PKC- mediated phosphorylation in adhesion and myelination. *J Cell Biol*. 2001;155:439-446.
13. Giese KP, Martini R, Lemke G, Soriano P, Schachner M. Mouse P0 gene disruption leads to hypomyelination, abnormal expression of recognition molecules, and degeneration of myelin and axons. *Cell*. 1992;71:565-576.
14. Filbin MT, Zhang K, Li W, Gao Y. Characterization of the effect on adhesion of different mutations in myelin P0 protein. *Ann N Y Acad Sci*. 1999;883:160-167.
15. Mandich P, Mancardi GL, Varese A, *et al*. Congenital hypomyelination due to myelin protein zero Q215X mutation. *Ann Neurol*. 1999;45:676-678.
16. Shapiro L, Doyle JP, Hensley P, Colman DR, Hendrickson WA. Crystal structure of the extracellular domain from P0, the major structural protein of peripheral nerve myelin. *Neuron*. 1996;17:435-449.
17. Liu Z, Wang Y, Yedidi RS, *et al*. Crystal structure of the extracellular domain of human myelin protein zero. *Proteins*. 2012;80:307-313.
18. Raasakka A, Ruskamo S, Kowal J, *et al*. Molecular structure and function of myelin protein P0 in membrane stacking. *Sci Rep*. 2019;9:642.

19. Grandis M, Acsadi AJ, Jain M, Kamholz J, Shy ME. Early and late onset mechanisms in CMT1B. In: *Third International Symposium on Charcot Marie Tooth Disorders*. Antwerp Belgium; 2004.
20. Raasakka A, Kursula P. How does protein zero assemble compact myelin? *Cells*. 2020;9:1832.
21. Shy ME. Peripheral neuropathies caused by mutations in the myelin protein zero. *J Neurol Sci*. 2006;242(1-2):55-66.
22. Shy M. Hereditary motor and sensory neuropathies related to MPZ (P0) mutations. In: Dyck PJ, Thomas PK, eds. *Peripheral neuropathy*. Elsevier/Saunders; 2005:1681-1716.
23. Saporta MA, Shy BR, Patzko A, *et al*. Mpzr98c arrests Schwann cell development in a mouse model of early-onset Charcot-Marie-Tooth disease type 1B. *Brain*. 2012;135(Pt 7): 2032-2047.
24. Pennuto M, Tinelli E, Malaguti M, *et al*. Ablation of the UPR-mediator CHOP restores motor function and reduces demyelination in Charcot-Marie-Tooth 1B mice. *Neuron*. 2008;57: 393-405.
25. Bai Y, Wu X, Brennan KM, *et al*. Myelin protein zero mutations and the unfolded protein response in Charcot Marie Tooth disease type 1B. *Ann Clin Transl Neurol*. 2018;5:445-455.
26. McCray BA, Scherer SS. Axonal Charcot-Marie-Tooth disease: From common pathogenic mechanisms to emerging treatment opportunities. *Neurotherapeutics*. 2021;18:2269-2285.
27. Delaglio F, Grzesiek S, Vuister GW, Zhu G, Pfeifer J, Bax A. NMRPipe: A multidimensional spectral processing system based on UNIX pipes. *J Biomol NMR*. 1995;6:277-293.
28. Lee W, Rahimi M, Lee Y, Chiu A. POKY: A software suite for multidimensional NMR and 3D structure calculation of biomolecules. *Bioinformatics*. 2021;37:3041-3042.
29. de la Torre JG, Huertas ML, Carrasco B. HYDRONMR: Prediction of NMR relaxation of globular proteins from atomic-level structures and hydrodynamic calculations. *J Magn Reson*. 2000;147:138-146.
30. Maciejewski MW, Schuyler AD, Gryk MR, *et al*. NMRbox: A resource for biomolecular NMR computation. *Biophys J*. 2017;112: 1529-1534.
31. Kirby N, Cowieson N, Hawley AM, *et al*. Improved radiation dose efficiency in solution SAXS using a sheath flow sample environment. *Acta CrystallogrD Struct Biol*. 2016;72:1254-1266.
32. Hopkins JB, Gillilan RE, Skou S. BioXTAS RAW: Improvements to a free open-source program for small-angle X-ray scattering data reduction and analysis. *J Appl Crystallogr*. 2017;50:1545-1553.
33. Petoukhov MV, Franke D, Shkumatov AV, *et al*. New developments in the ATSAS program package for small-angle scattering data analysis. *J Appl Crystallogr*. 2012;45:342-350.
34. Pettersen EF, Goddard TD, Huang CC, *et al*. UCSF Chimera—A visualization system for exploratory research and analysis. *J Comput Chem*. 2004;25:1605-1612.
35. Mirdita M, Schutze K, Moriwaki Y, Heo L, Ovchinnikov S, Steinegger M. Colabfold: Making protein folding accessible to all. *Nat Methods*. 2022;19:679-682.
36. Steinegger M, Soding J. MMseqs2 enables sensitive protein sequence searching for the analysis of massive data sets. *Nat Biotechnol*. 2017;35:1026-1028.
37. Jumper J, Evans R, Pritzel A, *et al*. Highly accurate protein structure prediction with AlphaFold. *Nature*. 2021;596:583-589.
38. Meng EC, Pettersen EF, Couch GS, Huang CC, Ferrin TE. Tools for integrated sequence-structure analysis with UCSF Chimera. *BMC Bioinformatics*. 2006;7:339.
39. Krissinel E, Henrick K. Inference of macromolecular assemblies from crystalline state. *J Mol Biol*. 2007;372:774-797.
40. Huang X, Pearce R, Zhang Y. EvoEF2: Accurate and fast energy function for computational protein design. *Bioinformatics*. 2020; 36:1135-1142.
41. Cao H, Wang J, He L, Qi Y, Zhang JZ. DeepDDG: Predicting the stability change of protein point mutations using neural networks. *J Chem Inf Model*. 2019;59:1508-1514.
42. Kozakov D, Hall DR, Xia B, *et al*. The ClusPro web server for protein-protein docking. *Nat Protoc*. 2017;12:255-278.
43. Konarev PV, Volkov VV, Sokolova AV, Koch MHJ, Svergun DI. PRIMUS: A windows PC-based system for small-angle scattering data analysis. *J Appl Crystallogr*. 2003;36:1277-1282.
44. Plotkowski ML, Kim S, Phillips ML, Partridge AW, Deber CM, Bowie JU. Transmembrane domain of myelin protein zero can form dimers: Possible implications for myelin construction. *Biochemistry*. 2007;46:12164-12173.
45. Dong H, Sharma M, Zhou HX, Cross TA. Glycines: Role in alpha-helical membrane protein structures and a potential indicator of native conformation. *Biochemistry*. 2012;51:4779-4789.
46. Senes A, Gerstein M, Engelman DM. Statistical analysis of amino acid patterns in transmembrane helices: The GxxxG motif occurs frequently and in association with beta-branched residues at neighboring positions. *J Mol Biol*. 2000;296:921-936.
47. Sanmaneechai O, Feely S, Scherer SS, *et al*. Genotype-phenotype characteristics and baseline natural history of heritable neuropathies caused by mutations in the MPZ gene. *Brain*. 2015;138: 3180-3192.
48. Veneri FA, Prada V, Mastrangelo R, *et al*. A novel mouse model of CMT1B identifies hyperglycosylation as a new pathogenetic mechanism. *Hum Mol Genet*. 2022;31:4255-4274.
49. Dill KA. Dominant forces in protein folding. *Biochemistry*. 1990; 29:7133-7155.
50. Das I, Krzyzosiak A, Schneider K, *et al*. Preventing proteostasis diseases by selective inhibition of a phosphatase regulatory subunit. *Science*. 2015;348:239-242.
51. Ron D, Walter P. Signal integration in the endoplasmic reticulum unfolded protein response. *Nat Rev Mol Cell Biol*. 2007;8:519-529.
52. Fridman V, Sillau S, Bockhorst J, *et al*. Disease progression in Charcot-Marie-Tooth disease related to MPZ mutations: A longitudinal study. *Ann Neurol*. 2023;93:563-576.
53. Pisciotta C, Neuropathy SM. Neuropathy. *Handb Clin Neurol*. 2018;148:653-665.
54. Shy ME, Jani A, Krajewski K, *et al*. Phenotypic clustering in MPZ mutations. *Brain*. 2004;127:371-384.
55. Inouye H, Tsuruta H, Sedzik J, Uyemura K, Kirschner DA. Tetrameric assembly of full-sequence protein zero myelin glycoprotein by synchrotron X-ray scattering. *Biophys J*. 1999; 76(1 Pt 1):423-437.
56. Hollingshead CJ, Caspar DL, Melchior V, Kirschner DA. Compaction and particle segregation in myelin membrane arrays. *J Cell Biol*. 1981;89:631-644.
57. Avila RL, D'Antonio M, Bachi A, *et al*. P0 (protein zero) mutation S34C underlies instability of internodal myelin in S63C mice. *J Biol Chem*. 2010;285:42001-42012.
58. Shy ME, Arroyo E, Sladky J, *et al*. Heterozygous P0 knockout mice develop a peripheral neuropathy that resembles chronic inflammatory demyelinating polyneuropathy (CIDP). *J Neuropathol Exp Neurol*. 1997;56:811-821.
59. Martini R, Zielasek J, Toyka KV, Giese KP, Schachner M. Protein zero (P0)-deficient mice show myelin degeneration in peripheral nerves characteristic of inherited human neuropathies. *Nat Genet*. 1995;11:281-286.
60. Howard P, Feely SME, Grider T, *et al*. Loss of function MPZ mutation causes milder CMT1B neuropathy. *J Peripher Nerv Syst*. 2021; 26:177-183.
61. Bai Y, Treins C, Volpi VG, *et al*. Treatment with IFB-088 improves neuropathy in CMT1A and CMT1B mice. *Mol Neurobiol*. 2022;59: 4159-4178.

62. Adams CJ, Kopp MC, Larburu N, Nowak PR, Ali MMU. Structure and molecular mechanism of ER stress signaling by the unfolded protein response signal activator IRE1. *Front Mol Biosci*. 2019;6:11.
63. Previtali SC, Quattrini A, Fasolini M, *et al*. Epitope-tagged P(0) glycoprotein causes Charcot-Marie-Tooth-like neuropathy in transgenic mice. *J Cell Biol*. 2000;151:1035-1046.
64. Shackleford G, Marziali LN, Sasaki Y, *et al*. A new mouse model of Charcot-Marie-Tooth 2J neuropathy replicates human axonopathy and suggest alteration in axo-glia communication. *PLoS Genet*. 2022;18:e1010477.
65. Filbin MT, Tennekoon GI. Homophilic adhesion of the myelin P0 protein requires glycosylation of both molecules in the homophilic pair. *J Cell Biol*. 1993;122:451-459.
66. Filbin MT, Tennekoon GI. The role of complex carbohydrates in adhesion of the myelin protein, P0. *Neuron*. 1991; 7:845-855.